Journal of Molecular Spectroscopy **197,** 85–99 (1999)
Article ID jmsp.1999.7896, available online at http://www.idealibrary.com on IDEAL®

High-Resolution FTIR and Millimeter-Wave Study of D_3SiF: The Ground, $\nu_3 = 1$, and $\nu_6 = 1$ and 2 States

N. Ben Sari-Zizi,* H. Najib,*,[1] H. Bürger,† E. B. Mkadmi,† Z. Kisiel,‡,§ M. Yu. Tretyakov,‡,[2] J. Demaison,‡ L. Margulès,‡ and P. Pracna¶

Laboratoire de Spectronomie Physique Appliquée, Faculté des Sciences, Université Mohammed V Agdal, BP 1014 Rabat, Morocco; †Anorganische Chemie, FB 9, Universität-Gesamthochschule, D-42097 Wuppertal, Germany; ‡Laboratoire de Physique des Lasers, Atomes et Molécules, UMR CNRS, Université de Lille 1, F-59655 Villeneuve d'Ascq Cedex, France; §Instytut Fizyki PAN, Al. Lotnikow 32/46, 02-668 Warsaw, Poland; and ¶J. Heyrovský Institute of Physical Chemistry, Dolejškova, CZ-18223 Prague 8, Czech Republic

Received February 17, 1999; in revised form May 6, 1999

The ν_6 (555.453 cm^{-1}), the ν_3 (888.899 cm^{-1}), and the very weak $2\nu_6$ infrared bands ($2\nu_6^{\mp 2}$ 1101.734 cm^{-1}, $2\nu_6^0$ 1100.102 cm^{-1}) for the ^{28}Si species of D_3SiF have been recorded with a resolution of 3.3, 2.4, and 5.0 $\times$ 10^{-3} cm^{-1}, respectively. Millimeter-wave spectra up to 640 GHz of D_3SiF in the ground, $\nu_3 = 1$, and $\nu_6 = 1$ and 2 states were measured. Ground state constants complete up to H constants including the K-dependent parameters A_0, D_K^0, and H_K^0 as obtained by the $\nu_6^{\pm 1}/2\nu_6^{\pm 2}$–$\nu_6^{\pm 1}/2\nu_6^{\mp 2}$ loop method were determined by a merge of 2388 ground state combination differences with 59 rotational data. The $\nu_3 = 1$ and $\nu_6 = 1$ and 2 levels appear to be unperturbed intervibrationally for the J and K values that could be accessed. However, $\Delta l = \Delta k = \pm 2$ and $\Delta l = \pm 2$, $\Delta k = \mp 4$ interactions affect the $\nu_6 = 1$ level while the $\nu_6 = 2$ levels undergo three interactions of $\Delta l = \Delta k = \pm 2$, $\Delta l = \pm 2$, $\Delta k = \mp 1$ and $\Delta l = \pm 4$, $\Delta k = \mp 2$ type. Typically, for the different bands, 2000–4000 pieces of infrared data augmented by 36–120 rotational data were fitted together. Owing to the weakness of the $2\nu_6$ band, the body of $\nu_6 = 2$ data was enlarged by energies that are deduced from the $2\nu_6$–ν_6 and ν_6 bands and which span in particular high K values. Comparison with available *ab initio* data derived from the harmonic and anharmonic force fields is made.

1. INTRODUCTION

Silyl fluoride, H_3SiF, is the lightest species among the silyl halides H_3SiX whose vibrational, rovibrational, and rotational spectra have been the subject of numerous high-resolution studies in the recent past (see, e.g., (*1*)). While the fundamental vibrations of H_3SiF have been investigated using high-resolution, near Doppler-limited infrared spectra (*2–5*), no such study had been performed for D_3SiF. Following very early work (*6*) there is only a low to medium resolution study dated from 1971 (*7*) by which the vibrational fundamentals were located, this careful study still marking the state of the art. Later, a microwave (MW) study of D_3SiF was undertaken (*8*), and three low J, K ground state transitions as well as five others within the $\nu_3 = 1$ and $\nu_6 = 1$ states have been measured. An experimental harmonic force field had been determined in which all existing data were used (*9*).

Interest in H_3SiF and its isotopic variety D_3SiF stems from the successful use of H_3SiF to pump far-infrared emissions with a CO_2 laser (*10–12*). The present project, ultimately directed toward the potential function and the accurate structure of H_3SiF, is of current interest. Both these latter molecular properties are closely related to rotational and rovibrational energy levels, which can be probed by high-resolution spectroscopy.

The most recent r_s and r_0 structures date back to 1976 (*9*) and 1986 (*13*), respectively, but it is well known that, for an accurate structure determination, equilibrium rotational constants of species with different off-axis substituents (i.e., D for H) are required (see, e.g., (*14*) for H_3SiBr/D_3SiBr). In fact such information derived from HD_2SiF and H_2DSiF had been used in the most recent structural work (*13*), in which also the axial rotational constant of D_3SiF could be estimated, $A_0 = 42\,711$ MHz (*1*). To obtain the required equilibrium rotational constants A_e and B_e of D_3SiF, all α_i^A and α_i^B values, $i = 1–6$, are needed. These are experimentally available only by a band-by-band analysis of all vibrational fundamentals.

The present task was to start a combined high-resolution infrared (IR) and millimeter-wave (MMW) investigation on the ground state and some low-lying fundamentals (ν_6, ν_3) of D_3SiF. Above all the determination of the axial rotational constant A_0 is a particular challenge, and we have chosen the now well-established "loop" method which uses a cold band ν_t, a hot band $(\nu_t + \nu_{t'})$–$\nu_{t'}$ and a combination $(\nu_t + \nu_{t'})^{\mp 2}$ as outlined in (*15*). This method was in fact first applied in the related molecule H_3SiCl (*16*) with $t = t' = 6$. For this purpose it was necessary to study in detail both ν_6 with the attached hot

Supplementary data for this article may be found on the journal home page (http://www.academicpress.com/jms).

[1] Permanent address: Département de Physique, Faculté des Sciences, Université Ibn Tofaïl, BP 133, Kénitra, Morocco.

[2] Permanent address: Institute of Applied Physics, Nizhnii Novgorod, Russia 603024.

0022-2852/99 $30.00

TABLE 1
Vibrational Wavenumbers (cm^{-1}) of $H_3{}^{28}SiF$ and $D_3{}^{28}SiF$

	$H_3{}^{28}SiF$	Ref.	$D_3{}^{28}SiF$	Ref.
ν_1 (A_1)	2206.717	*3*	1578 ± 2	*7*
ν_2 (A_1)	990.851	*4*	710.157	*18*
ν_3 (A_1)	875.010	*4*	888.899	This work
ν_4 (E)	2208.956	*3*	1615.62	*7*
ν_5 (E)	962.213	*4*	701.718	*18*
ν_6 (E)	729.528	*4*	555.453	This work
$\nu_3 + \nu_6$ (E)	1602.014	*2*	1435.696	*18*
$2\nu_6^0$ (A_1)	1457.998	*2*	1100.102	This work
$2\nu_6^{\mp 2}$ (E)	1460.788	*2*	1101.734	This work

band $2\nu_6^{\pm 2}$–$\nu_6^{\pm 1}$ and the overtone $2\nu_6^{\mp 2}$ interacting with $2\nu_6^0$. The present study, along with an analogous one of $D_3Si^{35}Cl$ (*17*), is the first that investigates the $2\nu_6^{\mp 2}/2\nu_6^0$ system of a trideuterated silyl (germyl, stannyl) halide. In H_3MX species, M = Si, Ge, Sn; X = F, Cl, Br, I, this overtone band is rather intense, and we expected this to be strong for D_3SiF, too, in analogy to H_3SiF (*2*). Although this analogy was in fact observed for the energy pattern, the intensity was found to be much smaller for the trideuterated species.

As is set out in Table 1 the vibrational energies of H_3SiF and D_3SiF differ significantly with the exception of ν_3, which, surprisingly, is shifted to higher energy by $+19$ cm^{-1} upon deuteration. According to Table 1, ν_6, ν_3, and $2\nu_6$ of D_3SiF on which we will report in the present contribution are fairly isolated from any other vibrational levels and may be considered in a first approximation as isolated bands, while ν_2 and ν_5 are almost degenerate. The study of the latter has also been completed and will be published elsewhere (*18*). The rovibrational energy patterns of ν_6, ν_3, $2\nu_6$, and also ν_2/ν_5 are urgently needed for the analysis of the wavenumber region > 1200 cm^{-1} because they take part in perturbers that affect the fundamentals ν_1 and ν_4 as well as overtones and combination levels in the mid and near infrared, keeping in mind that D_3SiF is a possible candidate to investigate local-mode behavior of the SiD stretching overtones.

H_3SiF and D_3SiF have been the subject of recent *ab initio* calculations of the harmonic (*19*) and anharmonic force fields (*20*, *21*). The numerous results obtained in these calculations are of great relevance for the present study, and they will be compared with experiment.

2. MATERIAL AND METHODS

2.1. Material

D_3SiF was prepared by reacting D_3SiI in a sealed glass ampoule at room temperature with SbF_3 for 2 h and was subsequently purified by repeated fractional condensation using a standard vacuum line. D_3SiI was prepared as described in (*22*). Since the $LiAlD_4$ had a deuteration enrichment of 99% our D_3SiF sample was unavoidably contaminated by ca. 3% of HD_2SiF. Moreover, since the fluorination was performed in a glass ampoule, traces of SiF_4 were formed which, owing to the large intensity of the ν_3 band of SiF_4 at 1032 cm^{-1}, became rather prominent when a long path cell was used to record the very weak $2\nu_6$ band centered at 1100 cm^{-1}. Finally, the large surface of the White-type cell made of glass caused some minor hydrolysis of D_3SiF on surfaces to yield $(D_3Si)_2O$, which has a strong, unstructured absorption at 1100 cm^{-1}. This was however eliminated ratioing the spectrum in this particular region against a 4 cm^{-1} resolution spectrum as background which was generated from the interferograms taken on the D_3SiF sample.

The Si isotopic abundance in the sample is 92% ^{28}Si, 4.7% ^{29}Si, and 3.3% ^{30}Si.

2.2. IR Spectra

Three spectra 1–3 covering the different bands were recorded in the present study. A Bruker 120 HR interferometer equipped with a globar source and a KBr beam splitter was used as detailed below.

Spectrum No.	1	2	3
Band	ν_6	ν_3	$2\nu_6$
Region (cm^{-1})	400–900	580–1080	750–2000
Resolution (1/MOPD)[a] (10^{-3} cm^{-1})	3.3	2.4	5.0
No. of scans	212	350	667
Detector	LHe–B:Si	LN_2–MCT600	LN_2–MCT800
Filter	—	>1200	>2400
Path length (cm)	28	28	400
Pressure (mbar)	3.0	0.5	8.0
Calibration, Region (cm^{-1}), (*23*)	H_2O, 500	CO_2, 670	H_2O, 1450
Recommended precision of calibration, (*24*)	$0.2 \cdots 0.5 \times 10^{-3}$	(1×10^{-3})	1×10^{-3}

[a] Maximum Optical Path Difference.

The recommended scaling factor for the H_2O lines in the 1450 cm^{-1} region, 0.999 999 770 (*24*), has not been applied to our calibration in view of the internal calibration that was applied. The mismatch of the *PPR* and *RRP* loops obtained, 0.190×10^{-3} cm^{-1}, however, compares well with the suggested scaling effect on $2\nu_6$ at 1100 cm^{-1}, 0.253×10^{-3} cm^{-1} (*24*). We estimate the wavenumber precision in the ν_3 and ν_6 region as 0.1×10^{-3} cm^{-1} and in the $2\nu_6$ region as 0.3×10^{-3} cm^{-1}.

2.3. Millimeter-Wave Measurements

The rotational spectrum of D_3SiF was observed in Lille up to 640 GHz. The MMW spectrum was measured up to 320 GHz with a spectrometer (*25*) using the harmonics of a phase-locked

klystron (74–80 GHz) as source and a superheterodyne detection. The submillimeter-wave spectrometer (*26*) used a Russian built BWO source emitting in the range 483–680 GHz phase-locked against a MMW frequency synthesizer working in the 78–118 GHz region. The absorptions were detected with a He-cooled InSb bolometer. The accuracy of the measurements is estimated to be better than 50 kHz.

3. DESCRIPTION OF THE IR SPECTRA AND ASSIGNMENTS

D_3SiF is a prolate symmetric top molecule which belongs to the point group C_{3v} and has three identical nuclei of spin $I_D = 1$. Therefore, the spin statistical weights are 11, 11, and 16 for the A_1, A_2, and E rovibrational levels, respectively. When the A_1–A_2 splitting is not resolved, this gives a spin statistical weight ratio of 22:16:16 for k–$l = 3p$, $3p + 1$, and $3p + 2$. The intensity alternance, although clearly evident, is therefore less pronounced than in the case of H_3MX molecules.

The six vibrational fundamentals, three of them nondegenerate of A_1 type, ν_1, ν_2, and ν_3, and three of them degenerate of E type, ν_4, ν_5, and ν_6, are given in Table 1.

The intensity of the ν_3 band is very large, and that of ν_6 is large, too, while the overtone band $2\nu_6$ is weaker than ν_6 by more than two orders of magnitude. Figure 1 gives overviews of the three bands that are the subject of the present study.

Around 550 cm^{-1} we identified in spectrum 1 the lowest fundamental ν_6 with two of its hot bands, $2\nu_6^{\pm 2}$–$\nu_6^{\pm 1}$ and $2\nu_6^0$–$\nu_6^{\pm 1}$, all being of perpendicular type. The hot bands exhibit respective integral intensities of about 14 and 7% relative to ν_6. Spectrum 2 shows around 890 cm^{-1} the ν_3 fundamental which is accompanied by hot bands, most prominently $(\nu_3 + \nu_6^{\pm 1})$–$\nu_6^{\pm 1}$ and $2\nu_3$–ν_3, the study of which was postponed for the moment because this will be undertaken simultaneously with the analysis of the related cold bands $\nu_3 + \nu_6^{\pm 1}$ and $2\nu_3$ near 1440 and 1770 cm^{-1}, respectively. Finally, in spectrum 3 around 1100 cm^{-1}, the weak overtone $2\nu_6$ with both its perpendicular and parallel components $2\nu_6^{\pm 2}$ and $2\nu_6^0$ was detected and assigned. Some coarse assignments of the survey spectra are given in Fig. 1.

3.1. The ν_6 Band

This band extends from 490–610 cm^{-1}. In the center it is governed by Q branches, successive Q branches being separated by ca. 1.5 cm^{-1}. The assignment was immediately recognized from its split $^PQ_3(J)$ branch which exhibits the first resolved doublet at $J = 28$ (see Fig. 2b where these split lines are shown), until at $J = 38$ they are obscured by the $^PQ_4(J)$ branch. The other Q branches were located from $^PQ_{21}$ to $^RQ_{21}$, all being J-degraded to small wavenumbers. The $^PQ_{15}$ branch is illustrated in Fig. 2a while the $^RQ_{15}(J)$ and $^RQ_{21}(J)$ branches are shown in Figs. 3a and 3b, respectively. Attached $\Delta J = \pm 1$ lines were assigned with the help of first lines $J'' = K''$ and by

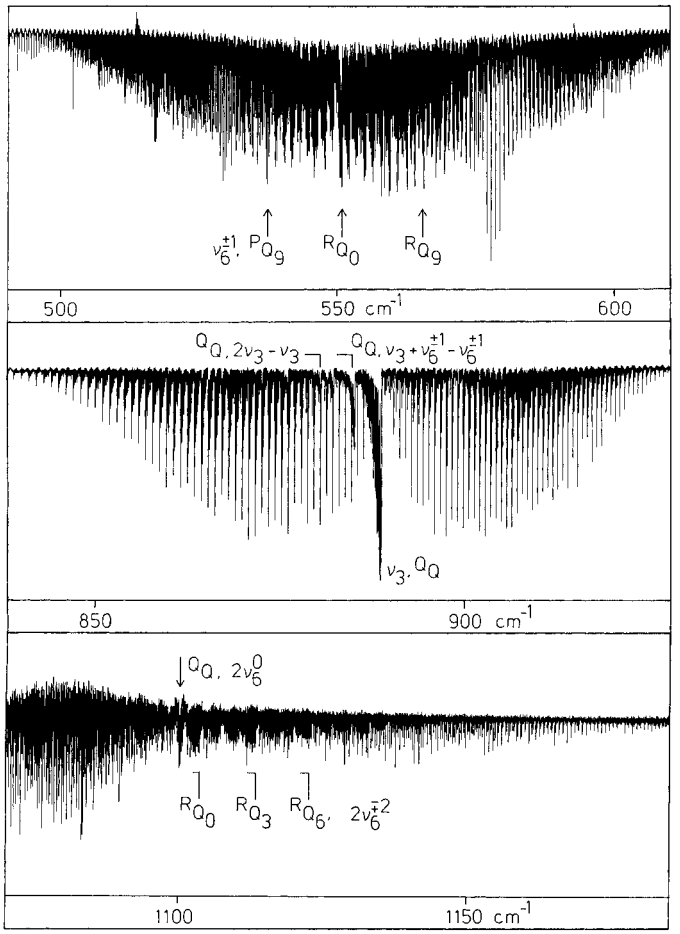

FIG. 1. Survey spectra of the ν_6 band (top), ν_3 band (middle), and $2\nu_6$ band (bottom) of D_3SiF. Some vibrational band centers and prominent Q branches are denoted.

rigorous use of ground state combination differences (GSCD) first obtained from the parameters of (*5*) and later improved using our own observations. Since the separation between successive subband origins, ca. 1.5 cm^{-1}, although significantly different from that of successive lines, ca. $2B \cong 0.8$ cm^{-1}, is on the same order of magnitude, some particular features appear in the ^PP and ^RR branches that should be mentioned. As is illustrated in Fig. 2a, the $^PP_{10}$ (*10*) line is followed by $^PP_7$ (*15*), $^PP_4$ (*20*), and $^PP_1$ (*25*) to low wavenumbers. This clustering of $^PP_{K-3n}(J + 5n)$ lines, $n = 0, 1, 2, \ldots$, was found in all $^PP_K(J)$ clusters, and there are three of such clusters A, B, and C for every $2B$ interval (see Fig. 2a). Whenever $J = K$, these clusters are particularly prominent because of the high intensity of the first $^PP_K(J)$ lines.

In contrast the strong $^RR_K(J)$ lines form only one single cluster consisting of $^RR_{K+n}(J - 2n)$ components, $n = 0, 1, 2, \ldots$. At low J this cluster evolves to small wavenumber with increasing K. As J increases the different ^RR lines approach and coincide for $^RR_{K+n}(34 - 2n)$, i.e., $^RR_3(28)$ etc., at 577.9 cm^{-1}, and thereafter K structure is again resolved and develops to

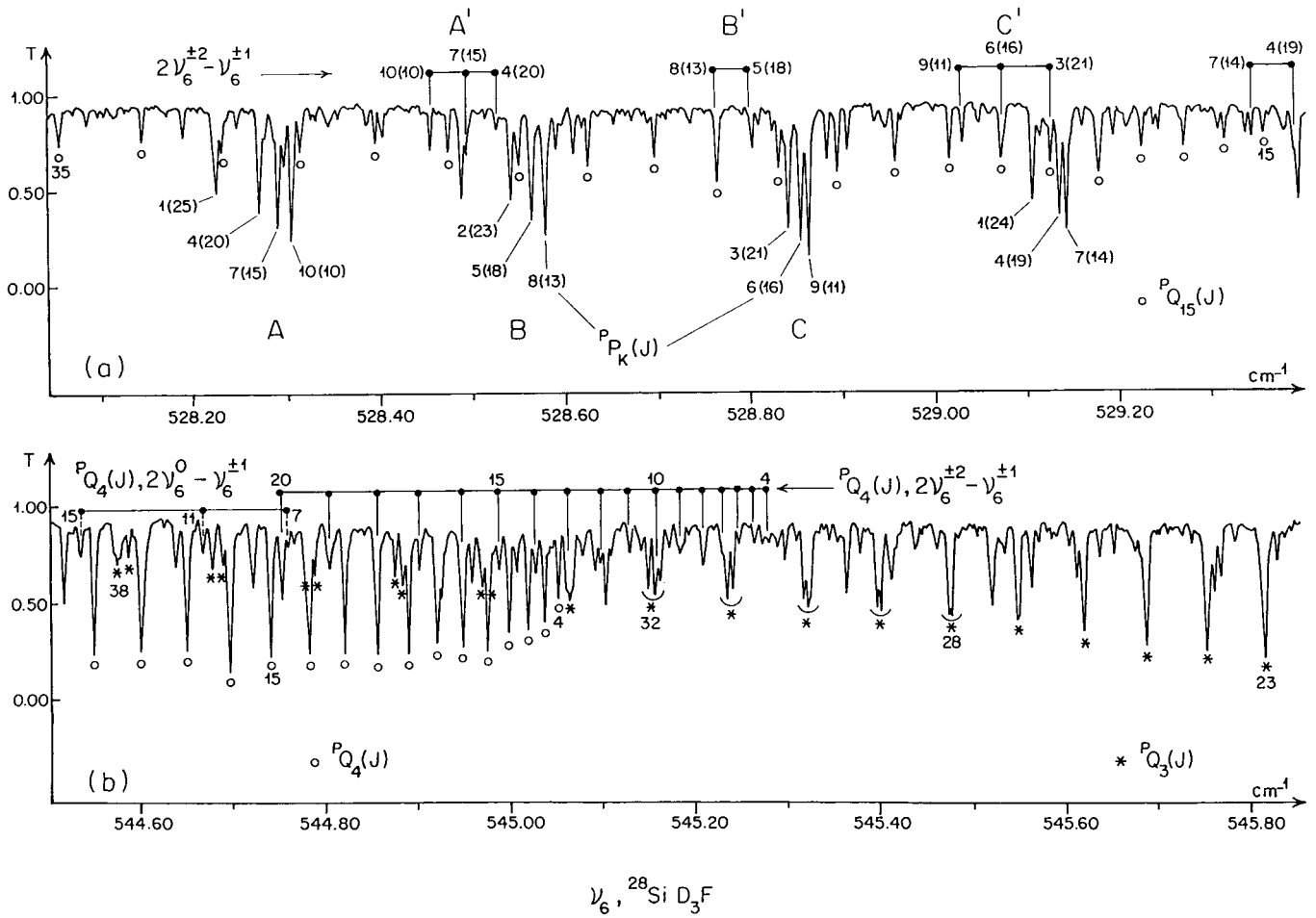

FIG. 2. Details of the ν_6 band system in the $\Delta K = -1$ branch region. (a) Bottom: Assignments of the $^PQ_{15}$ (J = 15–35) branch and of concomitant ^PP_K (J) lines of ν_6. Lines are labelled K'' (J''). Top: ^PP_K (J) lines of the $2\nu_6^{\pm2}-\nu_6^{\pm1}$ hot band. Note the line clustering A, B, C of ν_6 and A′, B′, C′ of the hot band. (b) Bottom: The $^PQ_3$ (J = 23–38) branch split for $J \geq 28$, and the $^PQ_4$ (J = 4–19) branch of ν_6. Top: The two $^PQ_4$ (J) branches of the hot bands. Right-hand side: $2\nu_6^{\pm2}-\nu_6^{\pm1}$. Left-hand side: $2\nu_6^{0}-\nu_6^{\pm1}$.

high wavenumber with increasing K (Fig. 3b). This particular behavior concentrates the whole bunch of ^RR lines to narrow intervals, which open windows that were essential for the detection of hot bands. The assignments of ν_6 were extended for the $^PP_K(J)$ lines up to $K = 24$ and for $^RR_K(J)$ lines up to $K = 30$, with $J_{max} = 62$, the total number of assigned lines reaching 4000.

3.2. *The $2\nu_6-\nu_6$ Hot Bands*

Concerning the $2\nu_6^{\pm2}-\nu_6^{\pm1}$ hot band, close inspection of the spectrum enables to detect, in the windows left by the cold $^RR_K(J)$ clusters, analogous clusters for other $^RR_K(J)$ series, which were supposed to belong to this strongest among the hot bands. The K numbering had to be evaluated with the assistance of the intensity alternation, with $K = 4, 7, 10, \ldots$, lines being reinforced.

The LSCD (lower state combination differences) calculated from (K, J) energy levels of $\nu_6 = 1^{+1}$ with the parameters given in Table 4 allowed to assign $^RQ_K(J + 1)$ branch lines for each observed $^RR_K(J)$ transition, which were found up to $K_{max} = 24$.

Shown for clarity on the top of the spectra, some $^RR_K(J)$ assignments of the hot band are reported in Fig. 3. They clearly indicate in Figs. 3a and 3b the same inversion occurring for the K-degradation within each cluster as for ν_6 when J increases.

In the $^RR_K(J)$ series of $2\nu_6^{\pm2}-\nu_6^{\pm1}$ the prominent cluster structure allowed to extend the assignments to high values of K. However, the extrapolation to small K values was often difficult, not only because of frequent overlaps but also due to the low intensity of low-K lines with large (J–K) values in relation to strong high-K lines where (J–K) is small.

In the $\Delta K = -1$ side of ν_6, many $^PQ_K(J)$ hot branches became evident after the more intense ones, corresponding to $K = 5, 8, 11, \ldots$, had been found by analogy with the previous $^RQ_K(J)$ branches. LSCD now applied to $\nu_6 = 1^{-1}$ sublevels unambiguously predicted the corresponding $^PP_K(J)$ lines.

In Fig. 2b the $^PQ_4(J)$ branch is shown while in Fig. 2a some

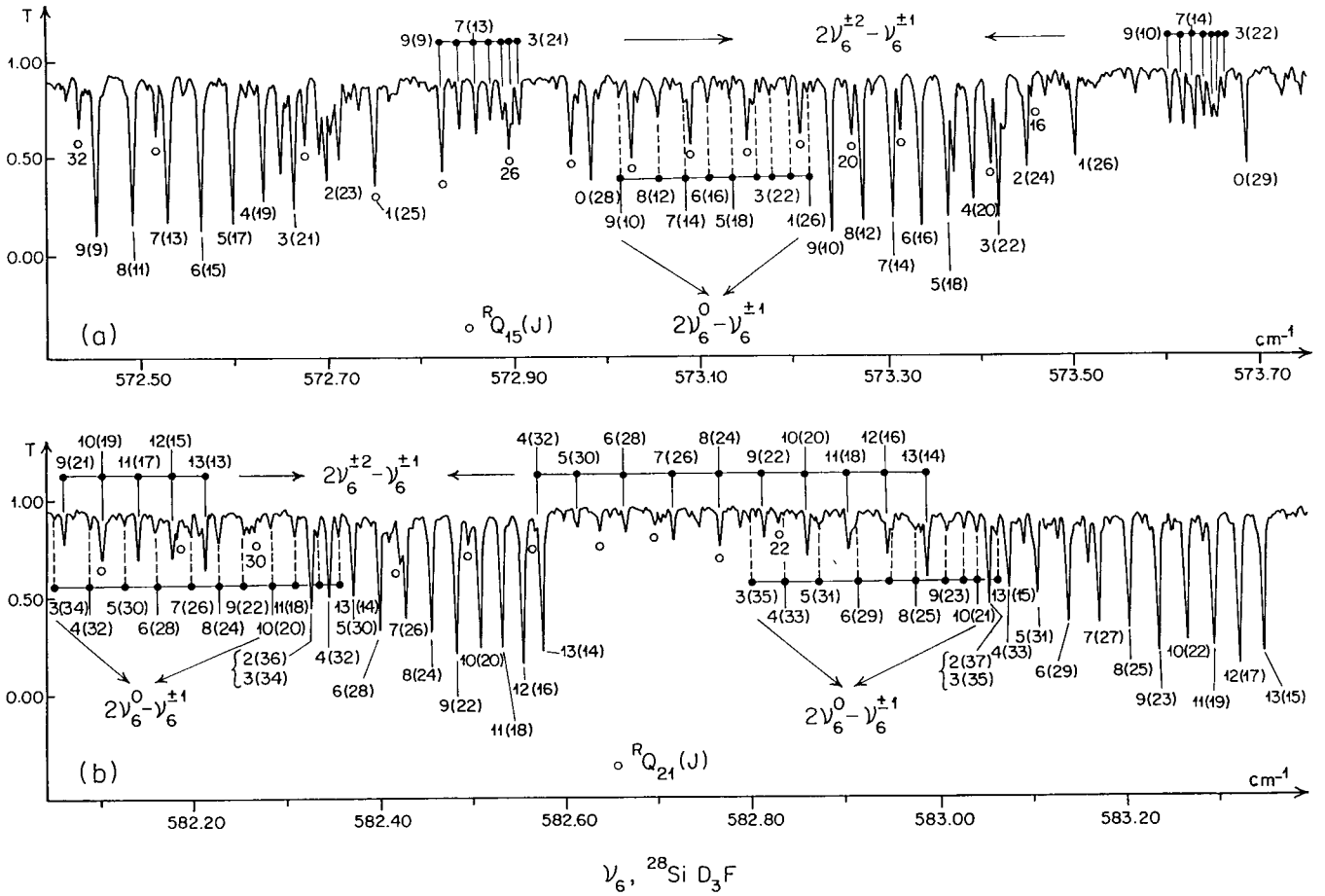

FIG. 3. Details of the ν_6 band system in the $\Delta K = +1$ branch region. (a) Bottom: Assignments of $^RR_K(J)$ lines of ν_6 and of the $2\nu_6^0-\nu_6^{\pm1}$ hot band. Top: $^RR_K(J)$ lines of the $2\nu_6^{\pm2}-\nu_6^{\pm1}$ hot band. (b) Bottom: The $^RQ_{21}(J = 22–32)$ branch region of ν_6 with $^RR_K(J)$ lines of ν_6 and of the $2\nu_6^0-\nu_6^{\pm1}$ hot band. Top: $^RR_K(J)$ lines of the $2\nu_6^{\pm2}-\nu_6^{\pm1}$ hot band. Note the inversion of K structure from trace (a) to trace (b).

hot $^PP_K(J)$ lines are assigned. These reveal again the same three-cluster structure denoted A′, B′, and C′ as described for ν_6.

In the dense central part of the spectrum we expect two $^PQ_2(J)$ and two $^RQ_1(J)$ branches since their respective lower levels had been found split in ν_6. While the latter was not seen, the former was in fact split for $J \geq 11$. This splitting could not be followed beyond $J = 13$ because of blending by the cold band.

Altogether a total of 1125 lines ($K_{max} = 24$, $J_{max} = 41$) belonging to the $2\nu_6^{\pm2}-\nu_6^{\pm1}$ hot band were assigned.

The weaker $2\nu_6^0-\nu_6^{\pm1}$ hot band was found with the help of the $2\nu_6^0$ and $\nu_6^{\pm1}$ lines for $K \leq 9$, the $2\nu_6^0$ component being indeed very weak. When the strongest $^RR_K(J)$ lines had been extracted, the assignment of the corresponding clusters could be extended to other K values, with $K = 2, 5, 8, \ldots$, lines being enhanced in intensity.

Figure 3 shows some $^RR_K(J)$ clusters of the $2\nu_6^0-\nu_6^{\pm1}$ hot band denoted by broken lines; in Fig. 3a one cluster comprising lines between $^RR_1(26)$ and $^RR_9(10)$ and in Fig. 3b two other clusters comprising lines from $^RR_{13}(14)$ to $^RR_3(34)$ and from $^RR_{13}(15)$ to $^RR_3(35)$, respectively, are displayed. The analogous behavior of the clusters with respect to those of ν_6 should be noted.

In spite of the weakness of the $\Delta K = -1$ side of $2\nu_6^0-\nu_6^{\pm1}$ some $^PQ_K(J)$ transitions were assigned. The $^PQ_4(J)$ branch is shown in Fig. 2b by broken lines. Eventually a total of 762 lines were assigned to this hot band, with $K_{max} = 15$ and $J_{max} = 38$.

3.3. The ν_3 Band

Because the ν_3 band behaves like a textbook example of a parallel band, only very few comments are given here. The central $^QQ_K(J)$ branches are congested with J and K increasing to the low wavenumbers. The $^QP_K(J)$ lines are nicely clustered, $K = 0$ and 1 lines not being resolved (Fig. 4a). Between the $J = 8$ and 9 clusters, the weak ^QQ branches belonging to $D_3{}^{29}SiF$ emerge. $^QR_K(J)$ lines are also clustered with regular K structure until at high K, lines are overlapped with the adjacent $(J + 1)$ cluster (Fig. 4b). Both in Figs. 4a and 4b the 11:8:8

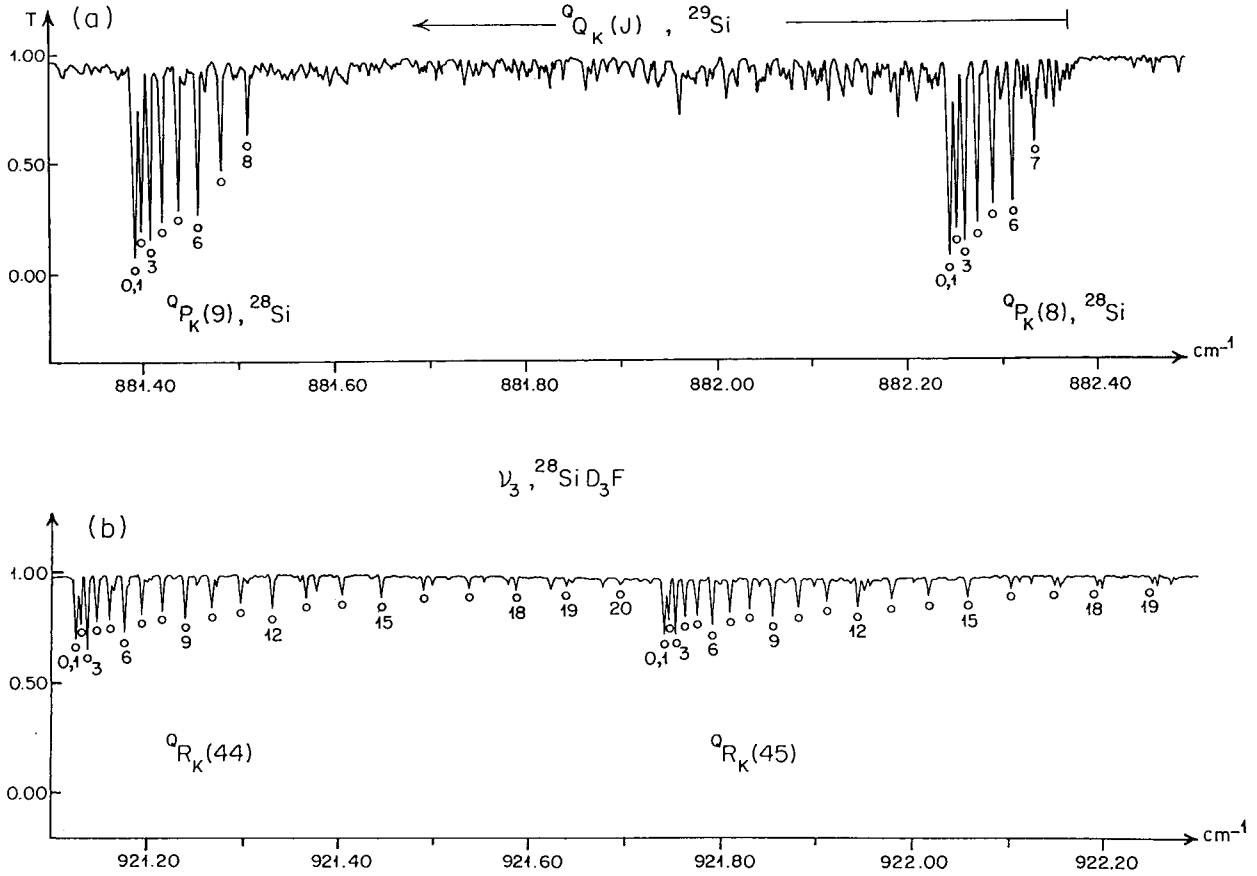

FIG. 4. J clusters of the ν_3 band. (a) The $^{Q}P_K$ ($J = 8, 9$) clusters with the weak ^{Q}Q branches belonging to the $D_3{}^{29}SiF$ species. (b) $^{Q}R_K$ ($J = 44, 45$) clusters.

intensity alternation for $K = 3p$ (p = integer) lines is clearly evident. More than 2200 lines were assigned and confirmed by GSCD reaching $K_{max} = 31$ and $J_{max} = 62$.

3.4. The $2\nu_6$ Bands

The $2\nu_6^{\mp 2}$ perpendicular component. The $\Delta K = +1$ side is more intense than the $\Delta K = -1$ side, this disproportion being more pronounced than in ν_6, and both sides remain intrinsically very weak. Moreover, due to the growing prominence of the R branches of SiF_4 below 1075 cm^{-1} (see Section 2) many of the weak $\Delta K = -1$ branch features are obscured (Fig. 1). Therefore, while our K assignments reached $K = 15$ for the $\Delta K = +1$ side, they ended at $K = 6$ on the $\Delta K = -1$ side, with only a few lines for $K \neq 3p$. Q branches of $2\nu_6^{\mp 2}$ are widely spread, well-resolved, extend to low wavenumber, and are ca. 3.3 cm^{-1} apart. No doubling of any line was observed; see, however, Section 3.2 for doubling of the $k = 1$, $l = -2$ level reached by $^{R}Q_0$ and $^{R}(P,R)_0$ transitions of $2\nu_6^{\mp 2}$.

We present in Figs. 5a and 5b a favorable portion with the $^{R}Q_3(J)$ and the $^{R}Q_{12}(J)$ branches accompanied by $^{R}R_K(J)$ lines in their proximity. Their $^{R}R_K$ ($J = K$) heads are the strongest lines, as demonstrated by the $^{R}R_2(2)$ line in Fig. 5a and the $^{R}R_9(9)$ transition in Fig. 5b. A total of 902 lines had been assigned, but they are not always of high quality. Only about 250 belong to the $\Delta K = -1$ side.

The $2\nu_6^0$ parallel component. The identification of this component was very difficult due to its very low intensity and the absence of any prominent features. Since its band center plays a key part in the analysis of the ($2\nu_6^{\mp 2}$, $2\nu_6^0$) system we have persistently searched for this band and finally found it by means of a Loomis–Wood program (*27*). Eventually we were able to assign 493 lines, covering $^{Q}R_K(J)$, $^{Q}P_K(J)$, and a few $^{Q}Q_K(J)$ with $K_{max} = 9$ and $J_{max} = 35$. Figure 5a illustrates the $^{Q}R_K$ ($J = 13$–16) lines whose assignments are indicated on the top and proves their low intensity in our spectra.

4. ANALYSIS

4.1. Ground State Parameters

4.1.1. The J-dependent constants. For the determination of the J-dependent ground state parameters (see Appendix Eq. [A1]) we had at our disposal the following items.

—A selection of 2388 unit-weighted GSCD from the ν_3 and ν_6 bands. A few of them which were based on evidently impure lines were given a weight of 0.1.

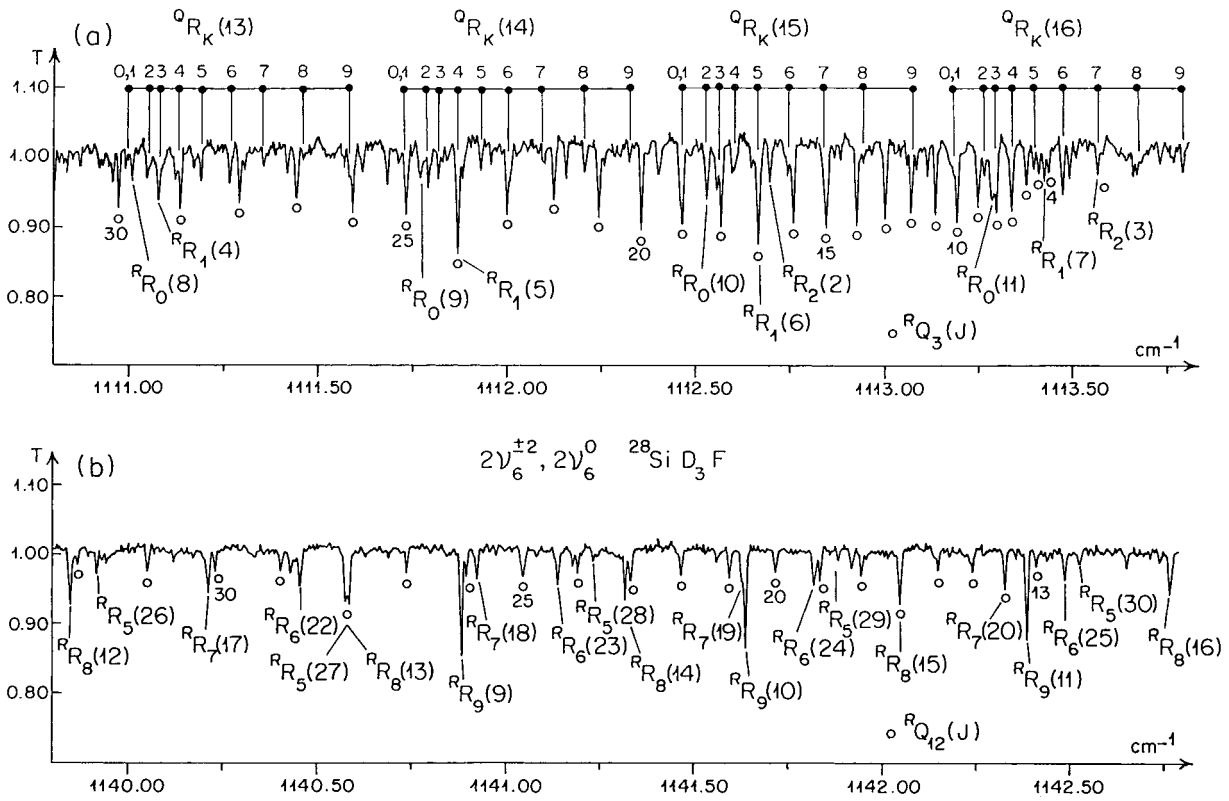

FIG. 5. Portions of the $2\nu_6$ band of D_3SiF. (a) Bottom: Assignments of the $^{R}Q_3$ ($J = 4$–30) branch of $2\nu_6^{\mp2}$ with some $^{R}R_{(K=0,1,2)}$ (J) lines. Top: The $^{Q}R_K$ ($J =$ 13–16) lines of $2\nu_6^0$. (b) Assignments of the $^{R}Q_{12}$ ($J = 13$–32) branch of $2\nu_6^{\mp2}$ with concomitant $^{R}R_{(K=4-9)}$ (J) lines.

—Three MW lines with $J = 0$ and 1 from Ref. (*8*) assigned a weight of 2000.

—Fifty-six MMW lines with $10 \leq J \leq 26$ of this work weighted 1000.

Given a precision of the unit-weighted GSCD of 93×10^{-6} cm^{-1} the weight assigned to the MW data would correspond to 2.1×10^{-6} cm^{-1} (60 kHz) and that of the MMW lines 2.9×10^{-6} cm^{-1} (90 kHz), which seems reasonable.

We have first fitted the infrared combination differences to the *J*-dependent GS constants which are gathered in the first column of the upper part of Table 2. Thereafter we merged all the available data and we obtained an improved set of GS parameters (Table 2, columns 2 and 3). Both sets are consistent within 3σ of the (poorer) GSCD data (4σ for H_{KJ}). The new B_0 parameter quoted in columns 2 and 3 of Table 2 supersedes the best previously available value, 12 253.141(5) MHz (*8*), by about one order of magnitude in spite of the correlation with (previously neglected) centrifugal distortion terms, which increase the standard deviation of the present value.

The ground state parameters reported in Table 2, column 2, have been held fixed in the fits that are outlined in the following sections. The results of the merged GS fit are gathered in Table S1 which was deposited as supplementary material.[3]

4.1.2. The K-dependent GS constants. Combining attached lines coming from the ν_6 fundamental, the $2\nu_6^{\mp2}$ overtone and the $2\nu_6^{\pm2}$–$\nu_6^{\pm1}$ hot band according to the *RRP* and *PPR* loops outlined in Ref. (*15*), the *K*-dependent GS constants (A, D_K, and H_K) have been determined employing a total of 245 $\Delta(K, J) = F(K, J) - F(K–3, J)$ differences. Although the hot band $2\nu_6^{\pm2}$–$\nu_6^{\pm1}$ and of course $\nu_6^{\pm1}$ would have permitted the use of a much larger stock of useful transitions, our body of $\Delta(K, J)$ data was limited to the $K = 3$–18 range by the restricted set of transitions of the weak $2\nu_6^{\mp2}$ partner, which is dictated by the limited assignments spanning only $-6 \leq K\Delta K \leq 15$.

Before fitting these $\Delta(K, J)$ differences we first checked the coherence of the calibration applied to spectra 1 and 2. Linking the ν_6 and $2\nu_6^{\pm2}$–$\nu_6^{\pm1}$ data from spectrum 1 with the $2\nu_6^{\mp2}$ data from spectrum 2 might introduce a mismatch which had to be evaluated beforehand. One way is to use the $2\nu_6^0$–$\nu_6^{\pm1}$ hot band,

[3] Lists of observed and calculated ground state combination differences and rotational and vibrational transition wavenumbers or upper state energies (161 pp.) have been deposited as supplementary material and may be obtained from Fachinformationszentrum Karlsruhe, D-76344 Eggenstein–Leopoldshafen, Germany, on submission of the names of the authors, the literature reference, and the registry number IRD-10092.

TABLE 2
Ground State Parameters of $D_3{}^{28}SiF$

	IR data only (cm^{-1})	(IR + MMW) data (cm^{-1})	(MHz)
B_0	0.408 720 775(83)	0.408 720 529(32)	12253.13320(96)
D_J^0	0.358 78(48) x 10^{-6}	0.358 719(31) x 10^{-6}	10.754 13(93) x 10^{-3}
D_{JK}^0	4.165 35(56) x 10^{-6}	4.165 36(17) x 10^{-6}	124.874 3(51) x 10^{-3}
H_J^0	1.440(81) x 10^{-13}	1.349(59) x 10^{-13}	0.004 04(18) x 10^{-6}
H_{JK}^0	1.506(14) x 10^{-11}	1.552 1(83) x 10^{-11}	0.465 3(25) x 10^{-6}
H_{KJ}^0	7.651(71) x 10^{-11}	7.235(23) x 10^{-11}	0.216 90(70) x 10^{-6}
No. of data[a]	2388	2388 + 59	
J_{max}, K_{max}, IR[a]	61/31	61/31	
J_{max}, K_{max}, MMW[a]		25/24	
σ, IR	0.093 x 10^{-3}		
σ, MMW		1.31 x 10^{-6}	39 x 10^{-3}
A_0	1.424 153 9(20)		42695.060(60)
D_K^0	2.075(17) x 10^{-6}		62.21(51) x 10^{-3}
H_K^0	-2.05(41) x 10^{-10}		-6.1(12) x 10^{-6}
No. of data[a]	245		
$\Delta(K, K-3)$[a]	$3 \le K \le 18$		
σ x 10^3	0.474		

(a): Dimensionless.
Errors given between parentheses are one standard deviation expressed in units of the last digit quoted.

as had been described in (*15*) and (*28*). We have selected about 100 apparently pure lines coming from $2\nu_6^0$ and $\nu_6^{\pm 1}$ and found that the calculated differences between corresponding wavenumbers and those observed for $2\nu_6^0$–$\nu_6^{\pm 1}$ were very small and almost random. Another way consists of comparing the $\Delta(K, J)$ differences for the same K coming from the *RRP* and *PPR* loops (*15*, *29*).

This method, when applied to apparently pure J lines but only for three common values of K (4, 5, 6), yielded systematic small deviations, whose average equals 0.000190 cm^{-1}. To compensate for this calibration mismatch we have subtracted 0.000095 cm^{-1} from all $\Delta(K, J)$ derived from the *PPR* path and added 0.000095 cm^{-1} to all $\Delta(K, J)$ belonging to the *RRP* path. The major source for this apparent calibration mismatch is the abovementioned small error in the H_2O calibration lines in the 1450 cm^{-1} region (*24*).

Now we can separate $\Delta(K, J)$ differences into a purely K-dependent term $\delta_1(K)$ and a small term $\delta_2(K, J)$ involving only J-dependent parameters according to Refs. (*30*) and (*2*):

$$\Delta(K, J) = \delta_1(K) - \delta_2(J, K) \quad \text{with}$$

$$\delta_1(K) = (A_0 - B_0)[K^2 - (K-3)^2] - D_K^0[K^4 - (K-3)^4] + H_K^0[K^6 - (K-3)^6]$$

$$\delta_2(J, K) = J(J+1)\{[D_{JK}^0 - H_{JK}^0 J(J+1)] \times [K^2 - (K-3)^2] - H_{KJ}^0[K^4 - (K-3)^4]\}.$$

D_{JK}^0, H_{JK}^0, and H_{KJ}^0 were taken as determined in the present work (Table 2).

A least-squares fit using the 245 $\delta_1(K)$ differences ($\sigma = 0.474 \times 10^{-3}$ cm^{-1}) yielded the results given in the lower part of Table 2, A_0 being deduced from $A_0 - B_0 = 1.015\ 433\ 4(20)$ cm^{-1}, employing B_0 from the present work (Table 2).

4.2. Excited State Parameters

Previous work on the $\nu_2/\nu_5/\nu_3/\nu_6$ vibrational tetrad of H_3SiF revealed the importance of *inter*vibrational interactions that may be of $(\Delta k$–$\Delta l) = 0$ (Fermi, Coriolis, and $\Delta l = \Delta k = \pm 2$

resonances) and $(\Delta k–\Delta l) = \pm 3$ type (α, $\Delta l = \pm 2$, $\Delta k = \mp 1$, and $\Delta k = 3$ resonances).

Although the strength of the rotational interactions in D_3SiF should be only slightly smaller than in H_3SiF, there are two reasons why such intervibrational interactions should be less important here. First, the step width of successive energy levels (neglecting Coriolis effects) is roughly $(A–B)(K^2–(K–1)^2) = (A–B)(2K–1)$. Since $(A–B) = 2.45\ cm^{-1}$ in H_3SiF but only 1.02 cm^{-1} in D_3SiF, the K and $k–l$ energy levels are much more compressed in D_3SiF than in H_3SiF. Moreover, the separation of adjacent vibrational levels is larger in D_3SiF than in H_3SiF for the vibrations under consideration (Table 1). On the other hand, we were able to probe much higher K, $(k–l)$ levels in D_3SiF than was possible in H_3SiF (*2, 4*) in correspondence to larger thermal population in the former. Thus one should be very careful when analyzing levels involving high-K values. K domains where $(\Delta k–\Delta l) = \pm 3$ interactions may be important are evident from Fig. 6, in which relevant K levels of ν_2, ν_3, ν_5, ν_6, and $2\nu_6$ are displayed. For the present cases the following $(\Delta k–\Delta l) = \pm 3$ interactions may be relevant:

(i) $v_6 = 1, \quad l_6 = +1, \quad K = 17,18 \leftrightarrow v_5 = 1,$
$l_5 = -1, \quad K = 12,13\ (\Delta l = \pm 2,\ \Delta k = \pm 5),$

(ii) $v_6 = 1, \quad l_6 = +1, \quad K = 23,24 \leftrightarrow v_2 = 1,$
$K = 19,20\ (\Delta l = \pm 1,\ \Delta k = \pm 4),$

(iii) $v_3 = 1, \quad K = 20, 21, 22 \leftrightarrow v_5 = 1,$
$l_5 = +1, \quad K = 24, 25, 26\ (\Delta l = \pm 1, \Delta k = \pm 4),$

(iv) $v_3 = 1, \quad K = 25, 26, 27 \leftrightarrow v_6 = 2,$
$l_6 = -2, \quad K = 20,21,22\ (\Delta l = \pm 2,\ \Delta k = \pm 5).$

In none of our data sets were we able to trace any effects due to the abovementioned possible intervibrational perturbations, mostly because the energy levels in question could not be probed to sufficiently high J values, the strength of supposed interactions increasing with $(J–k)$. This justifies to treat the ν_6, ν_3, and $2\nu_6$ bands as isolated systems.

4.2.1. The ν_3 band. A diagonal model up to sextic terms (see Eq. [A2]) was used to fit the ν_3 data with all GS constants constrained to those of Table 2. A least-squares program reported in (*31*) was used. The $v_3 = 1$ excited state parameters from fits of 2240 IR transitions (first column) and from a merge of these with 3 MW lines, Ref. (*8*), and 35 MMW transitions $(12 \le J \le 25)$ of this study, 25 of them weighted 2000 (column 2), are gathered in Table 3. The corresponding rms of $0.123 \times 10^{-3}\ cm^{-1}$ (IR) and $1.16 \times 10^{-6}\ cm^{-1}$, respectively, are satisfactory in view of the quality of the data and justify that ν_3 is really an isolated band. The observations, and their fits, are deposited in Table S2.

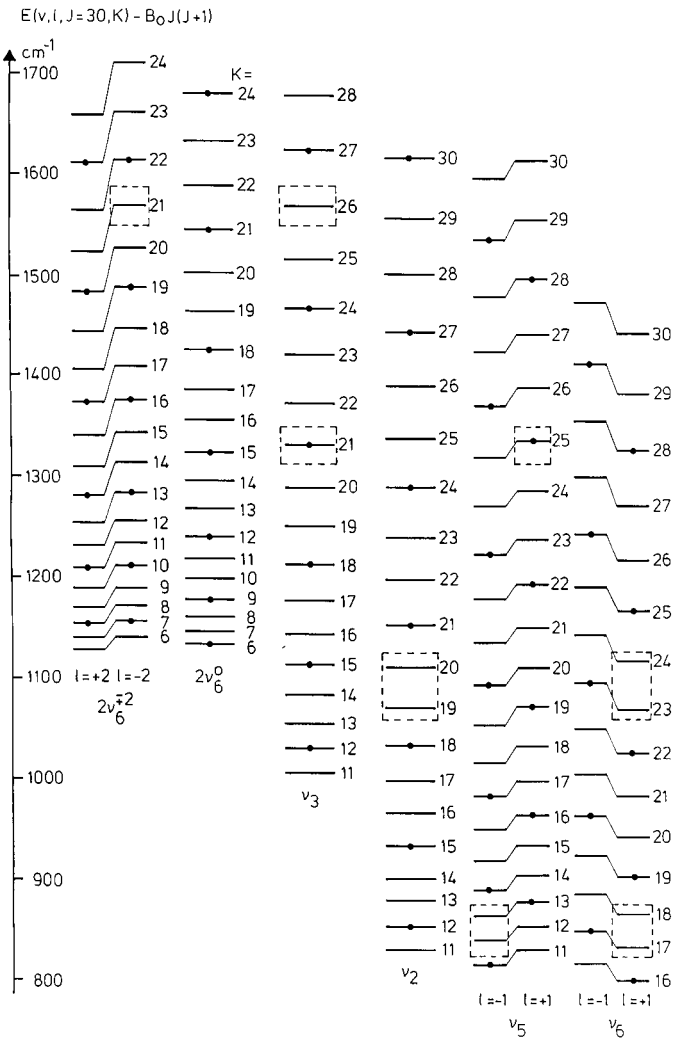

FIG. 6. Reduced $J = 30$ upper state energy levels labeled by their $K = |k|$ values of ν_6, ν_5, ν_2, ν_3, and $2\nu_6$. Levels with A_1A_2 symmetry ($k–l$ multiple of 3) are denoted by dots. kl domains which may undergo intervibrational interactions of $(k–l) = 3$ type are in hatched boxes.

4.2.2. The ν_6 band. The body of ν_6 data comprised almost 4000 unit-weighted IR observations and, in addition, 5 low J MW lines from Ref. (*8*) and 107 MMW data lines $(8 \le J \le 25)$ of the present study, with 89 of them assigned a weight of 2000.

Beyond the diagonal terms of the energy matrix (Eq. [A3]) the ν_6 band required two additional terms. One of these accounted for the splitting of the $kl = 1$ level reached by ${}^RQ_0$ and ${}^R(P,R)_0$ transitions ($l(2, 2)$ or $q_t^{(+)}$ resonance (Eq. [A4])) and a second interaction term (Eq. [A6]) describes the A_1A_2 splitting of the $kl = -2$ level which was resolved for $J \ge 27$ and increased to $14.4 \times 10^{-3}\ cm^{-1}$ at $J = 40$. We verified by means of GSCD that this splitting is not associated with any splitting of the $K = 3$ ground state level (*32*). The splitting of the $kl = -2$ level was accounted for by a direct term t ($\Delta l = \pm 2$, $\Delta k = \mp 4$ resonance). Introducing the term q_6, σ (Fit) of the IR data

TABLE 3
Parameters (cm^{-1}) of the $v_3 = 1$ State of $D_3{}^{28}SiF$

	IR data only	(IR + MMW data)
ν_0	888.898 812(11)	888.898 803 7(92)
A	1.423 777 8(98)	1.423 777 8(99)
B	0.406 564 103(29)	0.406 564 068(21)
$D_J \times 10^6$	0.350 621(19)	0.350 602(14)
$D_{JK} \times 10^6$	4.166 79(12)	4.166 66(10)
$D_K \times 10^6$	2.067(30)	2.067(30)
$H_J \times 10^{13}$	3.102(33)	3.076(27)
$H_{JK} \times 10^{11}$	1.750 9(38)	1.746 7(32)
$H_{KJ} \times 10^{11}$	7.235[a]	7.235[a]
$H_K \times 10^{10}$	-2.04(25)	-2.04(25)
No. of data[b]	2240	2240 + 38
J_{max}/K_{max}, IR[b]	62/31	62/31
J_{max}/K_{max}, MMW[b]		25/22
$\sigma \times 10^3$, IR	0.123	
$\sigma \times 10^6$, MMW		1.16 (35 kHz)

(a): Constrained to ground states value because not determined with significance.

(b): Dimensionless.

Errors given between parentheses are one standard deviation expressed in units of the last digit quoted.

dropped from 60×10^{-3} to 1.25×10^{-3} cm^{-1} and decreased further to 0.175×10^{-3} when also t was considered. The sign of q_6 with the convention of Ref. (*33*) is in agreement with the significant intensity perturbation already quoted in Ref. (*7*). A nonlinear least-squares fit program (*34*) was used. The results of the fits are given in Table 4, column 1 referring to the IR data only while column 2 quotes the results for the merged fit. The parameters of columns 1 and 2 generally agree within 3σ. Observed and calculated transition wavenumbers have been deposited in a supplementary Table S3.

4.2.3. The $v_6 = 2$ state. The $l = 0$ and $l = \mp 2$ components of the $v_6 = 2$ state were accessed by three independent sets of observations.

(i) IR data belonging to the cold bands $2\nu_6^0$ and $2\nu_6^{\mp 2}$.
(ii) IR data obtained from assignments of the hot bands $2\nu_6^0 - \nu_6^{\pm 1}$ and $2\nu_6^{\pm 2} - \nu_6^{\pm 1}$.
(iii) MMW data for 116 transitions (40 for $l = 0$ and 76 for $l_6 = \pm 2$ with $9 \leq J \leq 13$) within the $v_6 = 2$ vibrational level assigned a relative weight of 2000.

The fit was performed with a nonlinear least-squares program described previously (*35*). An advantage of this program is that it introduces by itself a relationship between coupling terms from $v_t = 1$ to $v_t = 2$ or 3 according to harmonic approximations. This means that the vibrational factor $v = (v_t \mp l_t + 2)(v_t \pm l_t)$ occurring in the off-diagonal elements (Eqs. [A4], [A5], and [A7]) which is 2 for $v_t = 1$ but $8^{1/2}$ for $v_t = 2$ had been automatically considered by the program. The fit was performed in three steps to finally take into account all transitions reaching, or within, the $v_6 = 2$ state.

First the $2\nu_6^0$ and $2\nu_6^{\mp 2}$ IR data were fitted together with the pure rotational observations.

The K levels of $2\nu_6^0$ are symmetrically located between the $k + 2$, $l = +2$, and $k - 2$, $l = -2$ sublevels of $2\nu_6^{\mp 2}$, and consideration of $l(2, 2)$ resonance reduces σ (Fit) of the diagonal model from 17.5×10^{-3} to 1.3×10^{-3} cm^{-1} for the $2\nu_6^0$ IR data, from 6.1×10^{-3} to 1.5×10^{-3} cm^{-1} for the $2\nu_6^{-2}$ IR data and from 25.1×10^{-3} to 7.0×10^{-3} cm^{-1} for the $2\nu_6^{+2}$ IR data. Levels interacting by $\Delta l = \pm 2$, $\Delta k = \mp 1$ resonance are

TABLE 4
Parameters (cm^{-1}) of the $v_6 = 1$ State of $D_3{}^{28}SiF$

	IR data only	(IR + MMW) data
ν_0	550.452 835(10)	550.452 865 9(83)
A	1.426 591 33(18)	1.426 590 74(15)
B	0.407 431 611(39)	0.407 431 503(27)
$D_J \times 10^6$	0.349 173(36)	0.349 111(28)
$D_{JK} \times 10^6$	4.244 38(32)	4.242 88(23)
$D_K \times 10^6$	2.425 38(61)	2.425 73(61)
$H_J \times 10^{14}$	7.95(90)	6.94(73)
$H_{JK} \times 10^{11}$	1.494(14)	1.434(11)
$H_{KJ} \times 10^{11}$	7.626(43)	7.564(41)
$H_K \times 10^{12}$	-2.063 1(76)	-2.057 0(76)
$A\zeta^z$	0.285 318 23(81)	0.285 316 10(71)
$\eta_J \times 10^6$	7.020 8(28)	7.011 2(20)
$\eta_K \times 10^5$	2.820 5(11)	2.819 9(11)
$\eta_{JJ} \times 10^9$	0[a]	0[a]
$\eta_{JK} \times 10^9$	0.140 5(24)	0.148 1(21)
$\eta_{KK} \times 10^9$	2.358(21)	2.362(21)
$q \times 10^3$	-1.102 489(71)	-1.102 487(59)
$q^J \times 10^9$	6.483(34)	6.469(30)
$q^K \times 10^7$	8.777(59)	8.904(57)
$t \times 10^9$	5.450(13)	5.456(13)
No. of data[b]	3897	3897 + 112
J_{max}/K_{max}, IR[b]	62/30	62/30
J_{max}/K_{max}, MMW[b]		25/25
$\sigma \times 10^3$, IR	0.175	
$\sigma \times 10^6$, MMW		4.4 (131 kHz)

(a): Constrained because not determined with significance.

(b): Dimensionless.

Errors given between parentheses are one standard deviation expressed in units of the last digit quoted.

TABLE 5
Parameters (cm^{-1}) of the $\nu_6 = 2^0$ and $2^{\mp 2}$ States of $D_3{}^{28}SiF$

	$\nu_6 = 2^0$		$\nu_6 = 2^{\mp 2}$
ν_0	1100.102 246(28)		1101.734 085(19)
A	1.428 859 62(70)		1.428 889 71(31)
B	0.406 189 34(80)		0.406 136 198 2(96)
$D_J \times 10^6$	0.341 163(87)		0.339 44(14)
$D_{JK} \times 10^6$	4.308 2(14)		4.336 38(95)
$D_K \times 10^6$	2.776 8(30)		2.749 4(13)
$H_J \times 10^{13}$		1.349[a]	
$H_{JK} \times 10^{11}$		1.552 1[a]	
$H_{KJ} \times 10^{11}$		7.235[a]	
$H_K \times 10^{10}$		-2.050 0[a]	
$A\zeta^z$			0.283 514 99(67)
$\eta_J \times 10^5$			1.494 4(37)
$\eta_K \times 10^5$			2.012 8(36)
$\eta_{JJ} \times 10^9$			0[b]
$\eta_{JK} \times 10^9$			0.148 1[c]
$\eta_{KK} \times 10^9$			2.362[c]
$F_{24} \times 10^7$			-1.80(36)
$q \times 10^3$		-1.079 09(67)	
$q^J \times 10^9$		1.84(82)	
$q^K \times 10^7$		8.24(92)	
$r \times 10^3$		1.240 6(28)	
$r^J \times 10^8$		-1.65(22)	
$r^K \times 10^8$		-3.98(51)	
No. of data[d]		3281 IR + 116 MW	
J_{max}/K_{max},IR[d]	38/15		41/24
J_{max}/K_{max}, MMW[d]	13/13		13/13
$\sigma \times 10^3$, IR		0.349	
$\sigma \times 10^6$, MMW		5.6 (168 kHz)	

(a): Constrained to the values of the ground state.
(b): Constrained because not determined with significance.
(c): Constrained to the values of ν_6, Table 4.
(d): Dimensionless.
Errors given between parentheses are one standard deviation expressed in units of the last digit quoted.

also close (Fig. 6) and the fit reached the experimental precision of the data, ca. 0.67×10^{-3} cm^{-1}, when this interaction (Eq. [A5]) was included, except for the ${}^RQ_0$ and ${}^R(P, R)_0$ branches, their $\nu_{obs} - \nu_{calc}$ being on the order of 3×10^{-3} cm^{-1} at $J = 25$. This systematic difference increasing with J required an additional parameter to account for $\Delta l = \pm 4$, $\Delta k = \mp 2$ interactions. The same situation had been met for $2\nu_6$ of H_3SiF (*2*). Introduction of the appropriate matrix element (see Eq. [A7]) removed all systematic deviations between observation and calculation, and ultimately an rms for 1219 nonzero weighted IR data belonging to $2\nu_6$ of 0.668×10^{-3} cm^{-1} was obtained. The 116 rotational transitions were fitted with $\sigma = 5.0 \times 10^{-6}$ cm^{-1} (150 kHz). Altogether the upper state fit requires one parameter linking levels with $(\Delta k–\Delta l) = \pm 3$ (r_t) and one connecting levels with $(\Delta k–\Delta l) = \pm 6$ (F_{24}). This selection of parameters is in agreement with the effort to avoid an ambiguity of the reduction of the effective Hamiltonian as discussed in Ref. (*36*) and applied to $\nu_6 = 2$ overtones (*37*).

Thereafter upper state energies $E(J, k, l)$ of the $\nu_6 = 2$, $l = 0$, and ± 2 states were formed by combining ground state energies obtained from the parameters of Table 2 with the addition of experimental, nonzero weighted transitions of ν_6 and of the hot band $2\nu_6^{\pm 2}–\nu_6^{\pm 1}$, respectively. No wavenumber corrections were applied. The obtained 1491 nonzero weighted experimental upper state energies which span predominantly high K values due to the easier detection of high-K hot band lines as outlined in Section 3.2 were fitted to $\nu_6 = 2$ parameters. In view of the composition of these data, F_{24} was set to zero, and q_t^J and q_t^K were constrained to the values of ν_6. The fit converged with 0.327×10^{-3} cm^{-1} for the IR data and $5.9 \times$

10^{-6} cm^{-1} (177 kHz) for the pure rotational data when η_{JK} and η_{KK} were constrained to the ν_6 values. The better quality of the energies determined in this fashion is—in spite of using two pieces of information, which increases the uncertainty of the data—a result both of the better resolution in the ν_6 region and the significantly higher intensities. Although the standard deviations of the different fits of $v_6 = 2$ parameters differ by a factor of two, we decided to assign the same weight to apparently pure $2\nu_6$ lines and energies obtained from unblended ν_6 and $2\nu_6$–ν_6 lines and to fit them together, the two bodies of data being complementary.

Finally the IR overtone transitions, the energies calculated from ν_6 and $2\nu_6$–ν_6, and the rotational data were fitted together. The results are gathered in Table 5. Observed and calculated rotational wavenumbers and excited state rovibrational energies have been deposited in a supplementary Table S4.

5. DISCUSSION

We have investigated both by high-resolution IR and by MMW spectroscopy the $D_3{}^{28}SiF$ molecule in the ground, $v_3 = 1$, $v_6 = 1$, and $v_6 = 2^0$ and $2^{\mp 2}$ states and determined thereof ground and excited states rovibrational parameters.

The ground state parameters up to sextic centrifugal distortion constants have been determined with high significance with the exception of H_K, $-2.05(41) \times 10^{-10}$ cm^{-1}, whose value is just five of its standard deviations and thus at the limit of unambiguous significance. The negative sign of H_K is indeed puzzling. However, the signs of H_J are also different for H_3SiF and D_3SiF, which does not contradict the empirical sign rule given in Ref. (*38*) that predicts a negative sign for prolate symmetric tops with $A/B > 4$. D_3SiF, $A/B = 3.48$, does not fulfill this condition which, to the contrary, H_3SiF does. We point out that H_J is analogously negative for H_3CF, but positive for D_3CF (*38*). Regrettably, *ab initio* calculations of the sextic constants from the anharmonic force field are only available for H_3SiF (*21*) while many other theoretical parameters of D_3SiF are given in Ref. (*20*). We compare experimental and *ab initio* molecular parameters of H_3SiF and D_3SiF in Table 6.

The agreement of experimental and *ab initio* quartic centrifugal constants is very good provided a scaling factor of 1.1–1.15 is applied to the *ab initio* values. The reasons for the systematic underestimation of *ab initio D* constants have been discussed in detail (*19*). The ground state rotational constants A_0 and B_0 are in very good agreement.

With regard to the anharmonicity constants x_{66} and g_{66}, the agreement is very favorable in view of the extremely small value of x_{66}. The vibration–rotation interaction constants α^A and α^B also agree within 20% with the exception of the small constant α_3^A, for which even the sign is at difference. We note a similarly large discrepancy for α_3^A for H_3SiF whose experimental value (1.414×10^{-3} cm^{-1}) (*4*) is 0.369×10^{-3} cm^{-1} larger than its *ab initio* prediction (*20*). The *ab initio* α constants are systematically smaller than the experimental values due to the *ab initio* overestimation of the ω_i's appearing in the denominator of the prefactor (*21*). The agreement for ζ_6^z is within 3%; the agreement of q_6 is within 10%. Compared to the earlier medium-to-low resolution study (*7*), we find agreement for $(\nu_3)^0$, $(\nu_6)^0$, $A\zeta_6^z$, and α_3^B, no other molecular parameters being really determined with significance in that study.

Expectedly the A_v and B_v values of the $l = 0$ and ± 2 components of $2\nu_6$ are similar, as are the D parameters, but to a lesser consistency among them and in comparison to their ground state values. In general, excited state quartic and sextic centrifugal distortion constants are reasonably close to their ground state values with the exception of H_J which varies by as much as a factor of 2 and thus takes the character of a fit parameter. Comparing the $2\nu_6$ rovibrational parameters A_0–A_v and B_0–B_v with those of ν_6 we find only small deviation from additive behavior, the experimental absolute values being

TABLE 6
Experimental and *Ab Initio* Molecular Parameters (cm^{-1}) of $H_3{}^{28}SiF$ and $D_3{}^{28}SiF$

	$H_3{}^{28}SiF$		$D_3{}^{28}SiF$	
ground state	exp.	*ab initio*	exp.[a]	*ab initio*
A	2.837 888[b]	2.855 4	1.424 154	1.431 9[c]
B	0.478 583	0.476 2	0.408 721	0.406 4[c]
$D_J \times 10^6$	0.527 7	0.458[d]	0.359	0.310[c, d]
$D_{JK} \times 10^6$	7.036	5.958[d]	4.165	3.539[c, d]
$D_K \times 10^6$	19.24[b]	16.52[d]	2.075	1.894[c, d]
$H_J \times 10^{12}$	-0.101[e]	+0.003 9[b]	0.135	-
$H_{JK} \times 10^{12}$	26.77[e]	21.80[b]	15.52	-
$H_{KJ} \times 10^{12}$	193.5[e]	142.8[b]	72.35	-
$H_K \times 10^{12}$	364.75[b, f]	364.75[b]	-205	-

$D_3{}^{28}SiF$, excited states	exp.[a]	*ab initio*
x_{66}	0.006 217(40)	0.06[a]
g_{66}	0.407 960(12)	0.38[b]
$\alpha_3^A \times 10^3$	0.376 2	-0.154[b]
$\alpha_3^B \times 10^3$	2.156 7	1.756[b]
$\alpha_6^A \times 10^3$	-2.436 8	-1.983[b]
$\alpha_6^B \times 10^3$	1.289 3	1.138[b]
ζ_6^z [g]	0.200 0	0.194 5[b]
$q_6 \times 10^3$	-1.102 5	-1.003[b]

(a): This work.
(b): Ref. (*21*).
(c): Ref. (*20*).
(d): Equilibrium values.
(e): Work by Demaison *et al.*, quoted in Ref. (*4*).
(f): Fixed to *ab initio* value.
(g): Dimensionless.

smaller by 3.5/2.9 (A_0–A_v) and 1.8/0.0% (B_0–B_v) for $2\nu_6^0/2\nu_6^{\mp 2}$ than their extrapolation from ν_6. The v-dependence of $A\zeta_6^z$ is small while that of η_J and η_K at first glance is surprisingly large (Tables 4 and 5). However, the parameters η_J and η_K depend on the reduction of the effective Hamiltonian used, which is not identical for ν_6 on the one hand and $2\nu_6$ on the other hand. However, the sum $\eta_{6J} + \eta_{6K}$ should be reduction-invariant (*36*), and this expectation is indeed perfectly fulfilled in our case, $(\eta_{6J} + \eta_{6K}) \times 10^{-5} = 3.522\ \text{cm}^{-1}$ ($\nu_6^{\pm 1}$) and $3.517\ \text{cm}^{-1}$ ($2\nu_6^{\mp 2}$). The interaction model chosen in $D_3Si^{35}Cl$ differs because there ν_3 and ν_6 are coupled by x,y-Coriolis resonance, and moreover, $2\nu_6$ is likewise coupled to $\nu_3 + \nu_6$, etc. Therefore no comparison with $D_3Si^{35}Cl$ seems to make sense.

Ab initio calculations predict also for D_3SiF a x,y-Coriolis interaction between ν_3 and ν_6, with $\zeta_{3,6}^y = 0.3483$ (*20*). In view of the larger difference of the band centers, ν_3–$\nu_6 = 333.5\ \text{cm}^{-1}$, it is not surprising that no indication for this resonance, i.e., unusually large (D_J''–D_J') and (D_{JK}''–D_{JK}') values, was found. Apparently $D_3{}^{28}SiF$ is a particularly favorable case of intervibrationally unperturbed rovibrational energy levels.

The present study which combines high-resolution IR data with novel MMW measurements provides accurate ground state parameters of $D_3{}^{28}SiF$ and gives a reliable picture of the $v_3 = 1$ and $v_6 = 1$ and 2 vibrationally excited states. Together with ν_2/ν_5, the analysis of which will be reported separately (*18*), these levels make up the ensemble of the lowest vibrationally excited states in the wavenumber domain $<1200\ \text{cm}^{-1}$. These levels take part in perturbers affecting the fundamental, combination, and overtone levels lying above $1200\ \text{cm}^{-1}$, and their careful analysis is therefore indispensable for ongoing work on other vibrational band systems.

APPENDIX

Diagonal and Off-Diagonal Matrix Elements of the Hamiltonian Operator

1. Diagonal matrix elements

Ground state energies were calculated using the formula

$$E(J, k) = B_0 J(J+1) + (A_0 - B_0)K^2 - D_J^0 J^2(J+1)^2 - D_{JK}^0 J(J+1)K^2 - D_K^0 K^4 + H_J^0 J^3(J+1)^3 + H_{JK}^0 J^2(J+1)^2K^2 + H_{KJ}^0 J(J+1)K^4 + H_K^0 K^6. \quad [A1]$$

where $K = |k|$.

Energies of A_1 vibrational states (ν_3, $2\nu_6^0$) were computed according the formula

$$E(v_s, J, k) = \nu_s^0 + (A_s - B_s)K^2 + B_s J(J+1) - D_J^s J^2(J+1)^2 - D_{JK}^s J(J+1)K^2 - D_K^s K^4 + H_J^s J^3(J+1)^3 + H_{JK}^s J^2(J+1)^2K^2 + H_{KJ}^s J(J+1)K^4 + H_K^s K^6. \quad [A2]$$

Energies of E vibrational states (ν_6, $2\nu_6^{\pm 2}$) were taken as

$$E(v_t, \ell_t, J, k) = \nu_t^0 + (A_t - B_t)K^2 + B_t J(J+1) - D_J^t J^2(J+1)^2 - D_{JK}^t J(J+1)K^2 - D_K^t K^4 + H_J^t J^3(J+1)^3 + H_{JK}^t J^2(J+1)^2K^2 + H_{KJ}^t J(J+1)K^4 + H_K^t K^6 - [2A\zeta_t^z - \eta_{tJ}J(J+1) - \eta_{tK}K^2 - \eta_{tJJ}J^2(J+1)^2 - \eta_{tJK}J(J+1)K^2 - \eta_{tKK}K^4]k\ell. \quad [A3]$$

2. Off-diagonal matrix elements

The $\ell(\pm 2, \pm 2)$ rotational resonance within $\nu_6^{\pm 1}$ and between the $2\nu_6^0$ and $2\nu_6^{\pm 2}$ components was treated by taking the off-diagonal elements

$$\langle v_t, \ell_t; J, k|\mathbf{H}|v_t, \ell_t \pm 2; J, k \pm 2\rangle = (-1/4)\{q_t + q_t^J J(J+1) + q_t^K[k^2 + (k \pm 2)^2]\} \times [(v_t \pm \ell_t + 2)(v_t \mp \ell_t)]^{1/2} F^{\pm}(J, k)F^{\pm}(J, k+1) \quad [A4]$$

with $F^{\pm}(J, k) = [J(J+1) - k(k \pm 1)]^{1/2}$.

The $\ell(\pm 2, \mp 1)$ rotational resonance between the $v_6 = 2^0$ and $v_6 = 2^{\pm 2}$ levels was treated according to the formula

$$\langle v_t, \ell_t \mp 1; J, k \pm 1|\mathbf{H}|v_t, \ell_t \pm 1; J, k\rangle = \{[r_t + r_t^J J(J+1)](2k \pm 1) + r_t^K[k^3 + (k \pm 1)^3]\}[(v_t \pm \ell_t + 2)(v_t \mp \ell_t)]^{1/2} F^{\pm}(J, k). \quad [A5]$$

The $\Delta\ell = \pm 2$, $\Delta k = \mp 4$ interaction (t resonance) related to the splitting of the $k\ell = -2$ sublevel of ν_6 had the following matrix element

$$\langle v_t = 1, \ell_t = -1; J, k+4|\mathbf{H}|v_t = 1, \ell_t = +1; J, k\rangle = \tfrac{1}{2} t_t F(J, k)F(J, k+1)F(J, k+2)F(J, k+3) \quad [A6]$$

with $F(J, k) = [J(J+1) - k(k+1)]^{1/2}$.

The $\Delta\ell = \pm 4$, $\Delta k = \mp 2$ interaction within $2\nu_6^{\pm 2}$ was given the following matrix element

$$\langle v_t, \ell_t; J, k|\mathbf{H}|v_t, \ell_t \mp 4; J, k \pm 2\rangle = F_{24}(v_t \mp \ell_t + 2)(v_t \pm \ell_t)F^{\pm}(J, k)F^{\pm}(J, k+1). \quad [A7]$$

ACKNOWLEDGMENTS

We thank Drs. A. Ceausu and G. Graner, Orsay (France), for valuable comments. Professor L. Halonen is thanked for the fit program Symtop. M.Yu.T. thanks the Russian Fund for Basic Research; E.B.M. acknowledges support by the Max-Planck-Gesellschaft zur Förderung der Wissenschaften e.V. The work in the Laboratoire de Spectronomie was carried out within the framework of the Moroccan "PARS Physique 25" project.

REFERENCES

1. H. Bürger and A. Rahner, *in* "Vibrational Spectra and Structure" (J. R. Durig, Ed.), Vol. 18, p. 217, Elsevier, Amsterdam, 1990.
2. A. Ceausu, G. Graner, H. Bürger, and P. Pracna, *J. Mol. Spectrosc.* **181**, 424–434 (1997).
3. H. Bürger and P. Schulz, *J. Mol. Spectrosc.* **125**, 140–153 (1987).
4. D. Papoušek, H. Bürger, A. Rahner, P. Schulz, H. Hollenstein, and M. Quack, *J. Mol. Spectrosc.* **195,** 263–280 (1999).

5. H. Bürger, P. Schulz, and J. Kauppinen, *J. Mol. Spectrosc.* **119**, 153–165 (1986).
6. C. Newman, J. K. O'Loane, S. R. Polo, and M. K. Wilson, *J. Chem. Phys.* **25**, 855–859 (1956).
7. A. G. Robiette, G. J. Cartwright, A. R. Hoy, and I. M. Mills, *Mol. Phys.* **20**, 541–553 (1971).
8. C. Georghiou, J. G. Baker, and S. R. Jones, *J. Mol. Spectrosc.* **63**, 89–97 (1976).
9. A. G. Robiette, C. Georghiou, and J. G. Baker, *J. Mol. Spectrosc.* **63**, 391–401 (1976).
10. P. B. Davies and D. P. Stern, *Int. J. Infrared Millimeter Waves* **3**, 909–916 (1982).
11. P. B. Davies, A. H. Ferguson, and D. P. Stern, *Infrared Phys.* **25**, 87–90 (1985).
12. P. B. Davies, D. P. Stern, and H. Jones, *Spectrochim. Acta A* **41**, 367–370 (1985).
13. J. L. Duncan, J. L. Harvie, D. C. McKean, and S. Cradock, *J. Mol. Struct.* **145**, 225–242 (1986).
14. J. Demaison, J. Cosléou, H. Bürger, and E. B. Mkadmi, *J. Mol. Spectrosc.* **185**, 384–391 (1997).
15. G. Graner and H. Bürger, *in* "Vibration-Rotational Spectroscopy and Molecular Dynamics. Advances in Quantum Chemical and Spectroscopical Studies of Molecular Structures and Dynamics," (D. Papoušek, Ed.), pp. 239–297, World Scientific, Singapore, 1997.
16. H. Bürger, G. Schippel, A. Ruoff, H. Essig, and S. Cradock, *J. Mol. Spectrosc.* **106**, 349–361 (1984).
17. A. Ceausu, G. Graner, H. Bürger, E. B. Mkadmi, and P. Pracna, *J. Mol. Spectrosc.* **194**, 128–141 (1999).
18. M. Badaoui, N. Ben Sari-Zizi, G. Graner, E. B. Mkadmi, H. Bürger, and P. Pracna, submitted for publication.
19. W. Schneider and W. Thiel, *J. Chem. Phys.* **86**, 923–936 (1987).
20. W. Thiel, Y. Yamaguchi, and H. F. Schaefer, *J. Mol. Spectrosc.* **132**, 193–206 (1988).
21. W. Schneider and W. Thiel, *Chem. Phys.* **159**, 49–66 (1992).
22. J. E. Gadhi, H. Bürger, and E. B. Mkadmi, *J. Mol. Spectrosc.* **191**, 311–315 (1998).
23. G. Guelachvili and K. Narahari Rao, "Handbook of Infrared Standards," Academic Press, San Diego, CA, 1986.
24. G. Guelachvili and 23 other authors, *Pure Appl. Chem.* **68**, 193–208 (1996).
25. J. Burie, D. Boucher, J. Demaison, and A. Dubrulle, *J. Phys. Paris* **43**, 1319–1325 (1982).
26. S. Bailleux, M. Bogey, H. Bolvin, S. Civis, M. Cordonnier, A. F. Krupnov, M. Yu. Tretyakov, A. Walters, and L. H. Coudert, *J. Mol. Spectrosc.* **190**, 130–139 (1998).
27. B. P. Winnewisser, J. Reinstädtler, K. M. T. Yamada, and J. Behrend, *J. Mol. Spectrosc.* **136**, 12–16 (1989).
28. A. Ceausu, G. Graner, H. Bürger, E. B. Mkadmi, J. Cosléou, and A. G. Lesarri, *J. Mol. Spectrosc.* **172**, 16–33 (1995).
29. R. Anttila, V.-M. Horneman, M. Koivuusari, and R. Paso, *J. Mol. Spectrosc.* **157**, 198–207 (1993).
30. J. Cheng and G. Graner, *J. Mol. Spectrosc.* **185**, 79–92 (1997).
31. C. Betrencourt-Stirnemann, G. Graner, D. E. Jennings, and W. E. Blass, *J. Mol. Spectrosc.* **69**, 179–198 (1978).
32. H. Bürger, H. Ruland, and L. Fusina, *Chem. Phys. Lett.* **268**, 249–257 (1997).
33. G. J. Cartwright and I. M. Mills, *J. Mol. Spectrosc.* **34**, 415–439 (1970).
34. (a) G. L. Caldow, L. O. Halonen, and J. Kauppinen, *Chem. Phys. Lett.* **101**, 100–105 (1983); (b) G. L. Caldow and L. O. Halonen, *Mol. Phys.* **46**, 223–237 (1982).
35. (a) A. Ceausu, G. Graner, H. Bürger, and P. Pracna, *J. Mol. Spectrosc.* **174**, 237–252 (1995). (b) P. Pracna, J. Demaison, G. Wlodarczak, A. Lesarri, and G. Graner, *J. Mol. Spectrosc.* **177**, 124–133 (1996).
36. E. I. Lobodenko, O. N. Sulakshina, V. I. Perevalov, and V. G. Tyuterev, *J. Mol. Spectrosc.* **126**, 159–170 (1987).
37. H. Harder, "15th International Conference on High Resolution Molecular Spectroscopy, Prague 1998," Contribution O2.
38. J. Demaison, R. Bocquet, W. D. Chen, D. Papoušek, D. Boucher, and H. Bürger, *J. Mol. Spectrosc.* **166**, 147–157 (1994).